Filatov, M. A.; Karuthedath, S.; Polestshuk, P. M.; Callaghan, S.; Flanagan, K. J.; Wiesner, T.; Laqaui, F.; Senge, M. O. (2018):
BODIPY-Pyrene and Perylene Dyads as Heavy-Atom-Free Singlet Oxygen Sensitizer.
ChemPhotoChem 2, 606–615. doi: 10.1002/cptc.201800020

BODIPY-pyrene and perylene dyads as heavy atom-free singlet oxygen sensitizers

Mikhail A. Filatov,*[a] Safakath Karuthedath,[b] Pavel M. Polestshuk,[c] Susan Callaghan,[a] Keith J. Flanagan,[a] Thomas Wiesner,[a] Frédéric Laquai[b] and Mathias O. Senge*[a]

Abstract: Dyads combining BODIPY as an electron acceptor and pyrene or perylene as electron donor subunits were prepared and studied their photophysical properties studied by steady-state and transient spectroscopy. Depending on the structure of the subunits and polarity of the media, the dyads show either bright fluorescence or photo-induced electron transfer (PeT) in solution. Charge-transfer (CT) states formed as a result of PeT and were found to yield triplet excited states of the BODIPY. In the presence of molecular oxygen, the dyads sensitize singlet oxygen ($^1O_2$) with quantum yields of up to 0.75.

Introduction

After the pioneering work of Kasha and Lewis[1] unveiled the origin of phosphorescence emission from organic molecules, research on triplet excited states became the subject of significant theoretical and experimental efforts. Triplet excited state chromophores have found applications in fields such as photodynamic therapy (PDT),[2] OLEDs,[3] photocatalysis,[4] bioimaging and sensing,[5] and photon upconversion.[6] Due to these advances and potential applications, methods to enhance intersystem crossing (ISC) in organic molecules are in high demand. One approach commonly used in the design of triplet sensitizers relies on the spin–orbit coupling in the presence of heavy atoms (typically halogens or transition metals) introduced into the chromophoric molecules, which leads to enhanced ISC (Fig. 1A). In recent years, alternative approaches toward the design of triplet sensitizers have attracted attention.[7]

Photo-induced electron transfer is a phenomenon commonly observed in dye molecules containing electron-donor and acceptor subunits.[8] The electronic structure of such molecules provides the possibility, that following light absorption, electron transfer from the donor unit to the acceptor takes places, creating a highly dipolar excited state; this is referred to as charge-transfer state (CT, Fig. 1B). It has been noted in many works that even in the absence of heavy atoms, CT states can undergo efficient ISC (so-called radical-pair intersystem crossing (RP-ISC))[9] or recombine to form local triplet excited states of either the donor or acceptor units (spin-orbit charge-transfer intersystem crossing (SOCT-ISC)).[10]

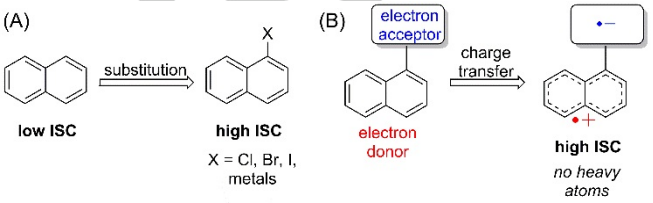

Figure 1. Approaches to enhance triplet excited state formation. (A) The heavy atom effect. (B) This work: enhanced ISC due to intramolecular charge-transfer.

Boron dipyrromethane (BODIPY) dyes[11][are widely applied as fluorophores and, if combined with an appropriate electron donor or acceptor units exhibit efficient PeT.[12] There have been a number of reports on long-lived triplet state formation in such dyads. For instance, BODIPYs with appended transition metal complexes, such as dyad **1**,[13] or dyads containing fullerene (**2**, Fig. 2),[14] have been shown to form triplet excited states of BODIPY without directly relying on the heavy atom effect. Similarly, BODIPY dyads containing quinone,[15] methylpyridinium or acridinium ion[16] (structures **3** and **4**, Fig. 2) subunits as electron donors and BODIPY dimers[17] demonstrated such properties. Recently, similar properties were observed for N,C-chelate organoboron dyes.[18]

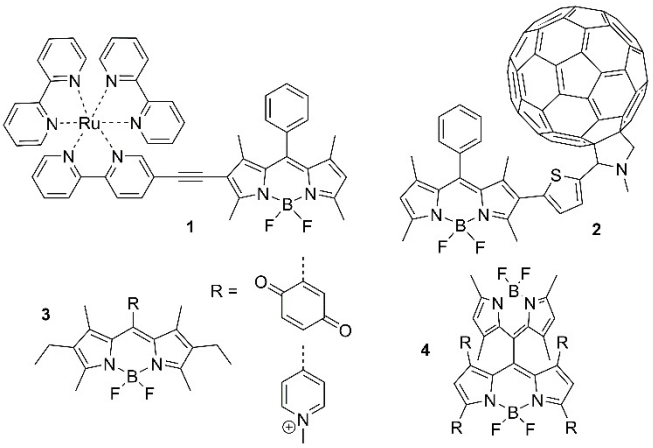

Figure 2. Examples of BODIPY dyads reported to generate triplet excited states through PeT mechanism.

[a] Dr. M. A. Filatov,† S. Callaghan, T. Wiesner, K. J. Flanagan, Prof. Dr. M. O. Senge
School of Chemistry, SFI Tetrapyrrole Laboratory, Trinity Biomedical Sciences Institute, 152-160 Pearse Street, Trinity College Dublin, The University of Dublin, Dublin 2, Ireland
E-mail: mikhail.filatov@dit.ie, sengem@tcd.ie
[b] Dr. S. Karuthedath, Prof. Dr. F. Laquai
KAUST Solar Center (KSC), Physical Sciences and Engineering Division (PSE), Material Science and Engineering Program (MSE)
King Abdullah University of Science and Technology (KAUST)
Thuwal 23955-6900, Kingdom of Saudi Arabia
[c] Dr. P. M. Polestshuk
Department of Chemistry
M. V. Lomonosov Moscow State University
Leninskie Gory, 1/3 Moscow 119991, Russia
† New address: School of Chemical and Pharmaceutical Science, Dublin Institute of Technology, Kevin Street, Dublin 8, Ireland

Supporting information (optical and NMR spectra, X-ray data) for this article is given *via* a link at the end of the document.

Employing PeT as a method of enhancing ISC has attractive advantages over the conventional heavy atom insertion strategy. E.g., halogenation of BODIPY results in rather low light-to-dark cytotoxicity ratios,[19] which is an obstacle for applications in PDT. This issue can be overcome with heavy atom-free BODIPYs. As we have recently shown, BODIPY-anthracene dyads (**BADs**, Fig. 3A) efficiently generate triplet states and singlet oxygen in biological media, while being non-toxic to cells in the absence of light irradiation.[20] Another advantage of PeT-mediated triplet sensitization relies on its medium polarity dependence. In non-polar environments (e.g., aromatic hydrocarbon solvents) the energy of CT states is much higher with respect to "local" excited states, as no stabilization through dipole-dipole interactions with solvent molecules can take place. As a result, PeT does not take place under such conditions and the dye behaves as a normal fluorophore, showing negligible ISC. Alternatively, in media of sufficient polarity, the CT state is stabilized and PeT becomes feasible. Recently in a proof-of-principle study, we demonstrated triplet sensitization switching in **BADs** by changing the media polarity in triplet-triplet annihilation photon up-conversion (TTA-UC).[21]

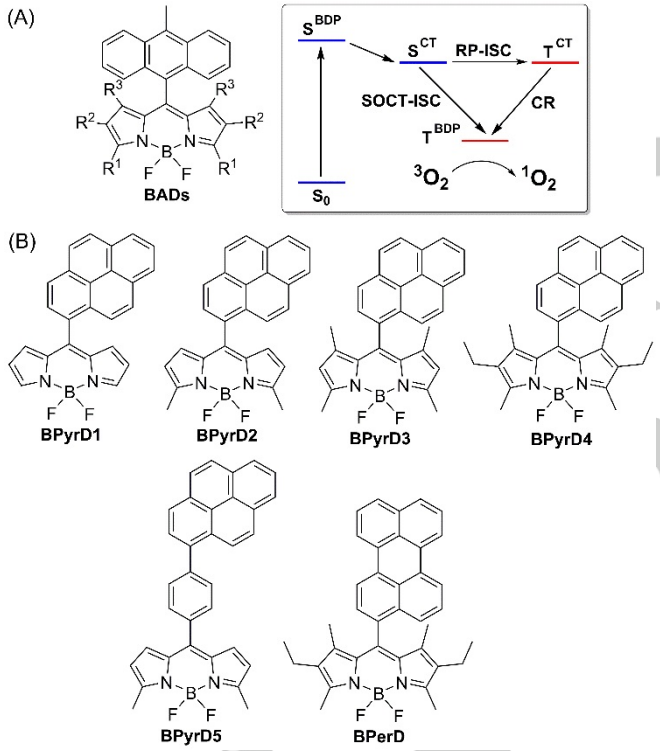

Figure 3. (A) Previously studied BADs forming triplet excited states via PeT and (B) dyads studied in this work. Inset: photophysical model for triplet excited states generation in dyads studied.

To develop applications for PeT-mediated triplet sensitization in BODIPYs the scope of such systems must be expanded and guidelines for tuning their photophysical behavior elucidated. The major limitation of the previously reported systems shown in Figure 2 is their synthetic availability. Recently, we performed a detailed study on triplet state generation in the readily accessible heavy atom-free **BADs**, based on various BODIPY scaffolds and anthracene subunits.[22] Here we describe dyads containing pyrene (**BPyrD1-4**) and perylene electron donors (**BPerD**, Fig. 3B). These are easily prepared in one-pot reactions and we have studied these dyads using steady-state and ultrafast transient absorption spectroscopy to confirm triplet state generation *via* PeT and the underlying kinetic parameters. Secondly, we investigated singlet oxygen generation of the dyads, which showed that using pyrene as an electron donor can provide higher Φ_Δ than previously reported **BADs**. The effect of solvent polarity and the substitution pattern of the BODIPY subunit on PeT and triplet state generation was examined. Structural information for various dyads was obtained by single-crystal X-ray crystallography. To rationalize the observed properties we employed quantum-mechanical calculations on the excited state electronic transitions in different types of dyads.

Results and Discussion

BODIPYs containing pyrene and perylene moieties have previously been reported in several works, however, ISC in the absence of heavy atoms has not been observed. Murgia *et al.* have shown that **BPyrD1** undergoes charge transfer in the excited state, which manifests in profound solvatochromism.[23] The emission quantum yields strongly decrease with increasing solvent polarity, while the emission maxima are red-shifted; this is typical for charge-transfer excited states. However, for dyads **BPyrD3**[24] and **BPyrD4**,[25] which are based on alkyl-substituted BODIPY scaffolds, the reported emission parameter are practically unaffected by solvent polarity and the dyads' photophysical properties are very similar to the corresponding 8-phenyl BODIPYs. This suggests that PeT in these dyads is governed by the alkyl-substitution pattern in BODIPY. Previous theoretical studies showed that the BODIPY frontier molecular orbital energies are strongly affected by the introduction of more alkyl groups.[26] We confirmed this by performing DFT calculations on the molecules shown in Figure 4.

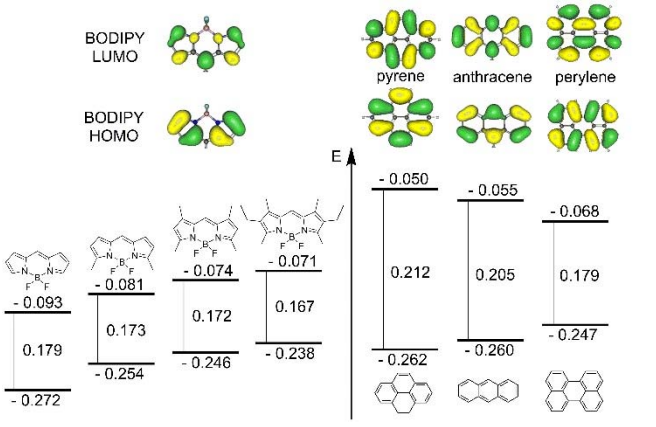

Figure 4. Calculated molecular orbital energies (in atomic units) corresponding to the HOMO and LUMO of BODIPY, pyrene, anthracene and perylene subunits.

Thus, to systematically investigate the PeT and triplet state generation processes in BODIPY pyrene dyads, we used four

BODIPY scaffolds with different alkyl substitution patterns, to tune the molecular orbital energy levels. Likewise, pyrene and perylene were chosen as electron donors because of their energy levels comparability to anthracene, which featured in our previous work.

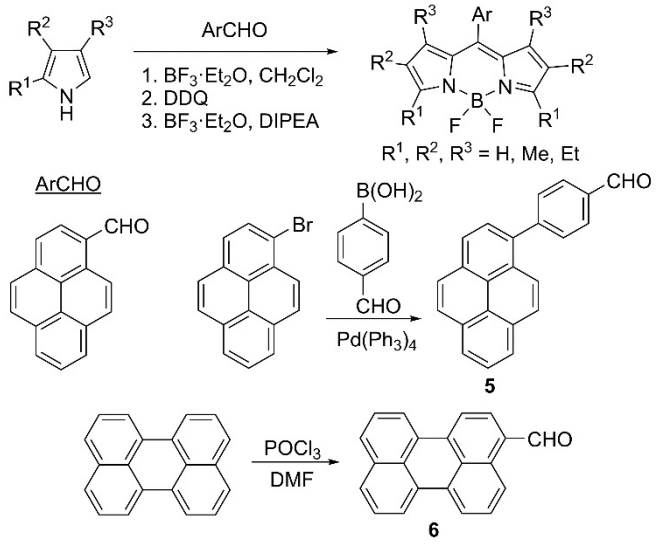

Scheme 1. Synthesis of the dyads studied.

The dyads were synthesized according to classic methods, using an acid-catalyzed condensation of the corresponding aldehydes with the respective pyrroles, followed by oxidation of intermediate dipyrromethanes with DDQ and boron insertion in the presence of base.[27] (Pyren-1-yl)benzaldehyde **5** was prepared *via* a Suzuki reaction between 1-bromopyrene and 4-formylphenylboronic acid. Perylene-3-carbaldehyde **6** was synthesized by the Vilsmeier formylation of perylene.

To examine the effects of the alkyl substituents and aromatic donor units on molecular geometry of the dyads, we obtained single crystals of the compounds synthesized, suitable for X-ray crystallography. We measured atom deviations from the least-squares-planes of the BODIPY and anthracene subunits (listed in Table 1), the carbon-carbon bond lengths of C8–C15 and the rotations around the C8–C15 bond, designated as *ψ* (Fig. 5). Additionally, in the packing arrangement, we evaluated the packing type (head-to-head or head-to-tail), solvent effects, and the formation of any halogen short contacts between fluorine and hydrogen atoms (bond lengths given with respects to H···F distance and angles are quoted for C–H···F).

In the BODIPY pyrene dyads, the ψ-angle was found to be close to 90°, irrespective of the substitution pattern in the BODIPY moiety. A similar conclusion is drawn from the C8–C15 carbon bond length. In the packing of **BPyrD1** (Fig. S5), a head-to-head dimer connected by a halogen bond between C5–H5···F14 (2.470(2) Å and 160.0(1)°) was observed. The packing of **BPyrD3** (Fig. S6) showed that the formation of head-to-tail aggregates is facilitated by the short contact between C22–H22···F13 (2.544(2) Å and 144.2(3)°). This appears to be a result of the sterically-hindered fluorine atoms due to the presence of the methyl substitution on C3 and C5, making this packing arrangement more favorable than the head-to-head dimer. The packing structure of **BPyrD4** (Fig. S7) showed two molecules in the asymmetric unit interacting with each other through one H···F contact at C35_1–H1H_1···F14_2 (2.576 (1) Å and 136.5(1)°).

Table 1. Selected structural details of rotations, bond length and planar distortions in studied dyads structures.

Compound	ψ (°)[a]	C8–C15 (Å)	ΔB (Å)[b]	ΔA/P (Å)[c]
BPyrD1	84.0 (1)	1.499(1)	0.071	0.023
BPyrD3	81.1(1)	1.490(1)	0.062	0.024
BPyrD4 [d]	87.5(2)	1.495(1)	0.018	0.020
	88.7(1)	1.498(1)	0.061	0.018
BPerD [d]	85.7(2)	1.495(1)	0.022	0.048
	84.5(2)	1.493(1)	0.016	0.095

[a] Dihedral angle between the mean planes of the BODIPY and meso-substituent. [b] Deviation of atoms from the mean plane of the BODIPY. [c] Deviation of atoms from the mean plane of the substituted pyrene or perylene. [d] Two independent molecules in the asymmetric unit and both structural factors are reported.

In **BPerD** (Fig. S8), the hydrogen atoms associated with the 6- and 7-positions of the perylene moiety formed bifurcated close contact to the fluorine of the BODIPY at 2.369(1) Å (173.2(1)°) for C20_2–H20_2···F13_1 and 2.449(1) Å (148.1(1)°) for C17_2–H17_2···F13_1. Additionally, the presence of the two independent molecules resulted in a mixture of head-to-head interactions coupled with a head-to-tail overlap in the unit cell.

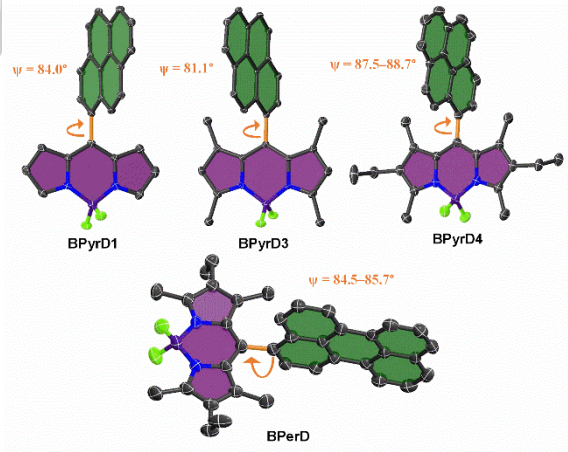

Figure 5. Single crystal X-ray crystallographic structural features of the dyads under investigation. Orange denotes the bond used to determine the C8–C15 bond length. ψ-Angle rotations were determined by measuring the dihedral angle between the pyrene (green) and BODIPY (purple) least-squares-plane. Thermal ellipsoids displacements show 50% probability, hydrogen atoms have been omitted for clarity.

The absorption and fluorescence emission parameters of the prepared dyads in different solvents are given in Table 2. Changing the solvent polarity was found to significantly impact the emission properties. The spectrum of **BpyrD1** (Fig. 6A) in

non-polar hexane (ε_r = 1.9) showed a fluorescence emission centered at 520 nm, characterized by a Stokes shift of 17 nm and an emission quantum yield of 0.161, which is in accordance with the characteristics of the corresponding 8-phenyl BODIPY.[11] This emission can be attributed to the $S_0 \rightarrow S_1$ transition in BODIPY, or "local emission" (LE) of the BODIPY chromophore exciton. Contrarily, in polar DMF (ε_r = 38.3), a new broad and structure-less band appeared at 715 nm, accompanied by a remarkable drop in emission intensity and quantum yield to 0.005 (Fig. 6A). This observation was reproduced in other solvents, showing a clear correlation between polarity, red shift of the emission, and its quantum yield. Such emission quenching in polar media is the signature of intramolecular electron transfer.[28] Red-shifted, broad emission bands correspond to the transition from the CT state, formed *via* intramolecular electron transfer into the ground state of the dyad.[29] Such emission is commonly very weak, consistent with the low quantum yields observed for **BpyrD1** in polar solvents. On the other hand, the emission observed for **BPyrD1** in toluene (Fig. 6B) can be interpreted as a mixture of fluorescence from the LE and CT state.

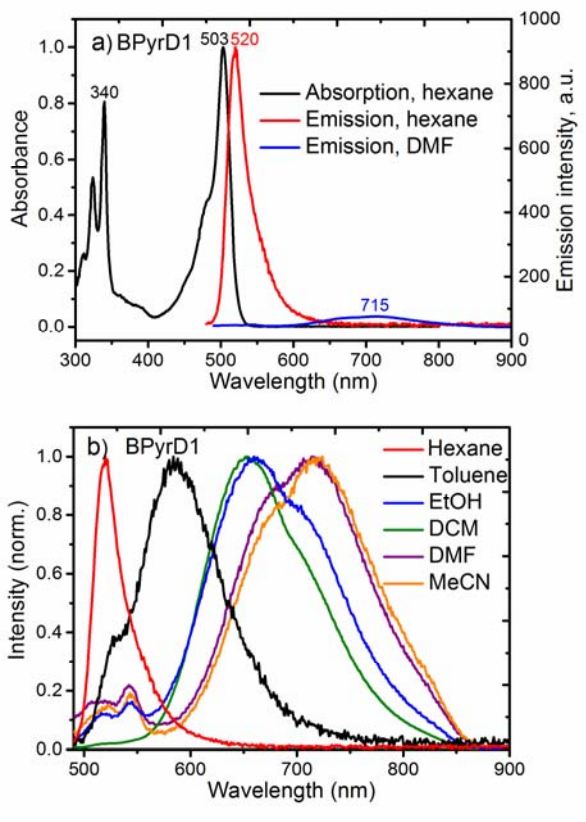

Figure 6. Absorption and emission spectra of **BPyrD1** in hexane and DMF (a), normalized emission spectra of **BPyrD1** in a range of solvents (b). The emission was excited at 470 nm for all samples.

As can be seen from Table 2, emission is less affected by the solvent polarity in dyads with alkyl substituents. **BPyrD2** showed substantially stronger emission in polar solvents and its LE emission was observed even in polar DMF. While **BPyrD3** still showed PeT, dyad **BPyrD4** was practically unaffected by the polarity, showing very similar fluorescence quantum yields in hexane and DMF (Fig. 7A). Dyad **BPyrD5**, in which the pyrene moiety is not directly linked to the BODIPY but separated *via* a phenylene bridge, exhibited properties consistent with PeT. In DMF, the CT emission was not observed (Fig. 7B). However, the observed LE emission was substantially weaker (Φ_{em} = 0.078) than in non-polar hexane (Φ_{em} = 0.226). This indicates, that, although PeT takes place in dyad **BPyrD5**, it is less efficient compared to the dyads with directly linked subunits. The rate of PeT is known to depend on the separation of the donor and acceptor subunits;[30] thus, introduction of the phenylene spacer in this dyad is likely to slow down the electron process. Similar characteristics were observed for dyad **BPerD**. Perylene has substantially higher MO energy levels compared to pyrene (see Fig. 4). These observations indicate that the PeT efficiency can vary to a large extent in these dyads and depends on the electronic coupling between the subunits.

Table 2. Steady-state spectroscopic data for **BPyrDs** and **BPerD** in various solvents.

Compound	Solvent[a]	λ_{abs}[b] (nm)	λ_{em}[c,d] (nm)	Φ_{em}[d,e]
BPyrD1	DMF	505	715	0.003
	DCM	505	654	0.021
	CH_3CN	501	717	0.002
	EtOH	503	660	0.003
	toluene	507	586	0.133
	hexane	503	520	0.161
BPyrD2	DMF	516	525, 630	0.028
	DCM	516	530	0.142
	CH_3CN	512	511, 652	0.017
	EtOH	513	524	0.063
	toluene	517	531	0.753
	hexane	514	526	0.747
BPyrD3	DMF	504	514	0.165
	DCM	505	514	0.805
	CH_3CN	501	509	0.126
	EtOH	502	511	0.651
	toluene	507	516	0.926
	hexane	503	513	0.967
BPyrD4	DMF	533	542	0.688
	DCM	537	544	0.761
	CH_3CN	531	540	0.608
	EtOH	534	542	0.695
	toluene	540	547	0.677
	hexane	538	542	0.755
BPyrD5	DMF	512	526	0.078
	DCM	513	527	0.187
	CH_3CN	508	523	0.04
	EtOH	510	522	0.136
	toluene	515	530	0.287
	hexane	511	526	0.226
BPerD	DMF	530	536	0.064
	DCM	531	541	0.176
	CH_3CN	527	533	0.063
	EtOH	529	536	0.073
	toluene	532	544	0.898
	hexane	529	540	0.924

[a] DMF – *N*,*N*-dimethylformamide, DCM – dichloromethane. [b] Absorption maxima corresponding to BODIPY chromophore are given. [c] The fluorescence was excited at the vibrational shoulder of the BODIPY absorption. [d] The fluorescence quantum yields were measured using fluorescein disodium salt as standard (Φ_{em} = 0.95 in 0.1 M NaOH). [d] Represents integral emission coming from LE and CT excited states.

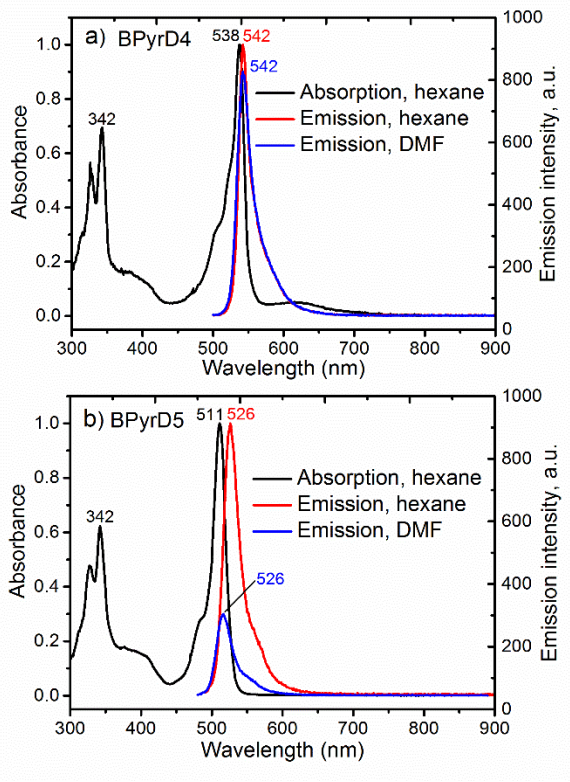

Figure 7. Absorption and emission spectra of **BPyrD4** (a) and **BPyrD5** (b) in hexane and DMF. The emission was excited at 490 nm for both dyads.

As has been noted in previous studies,[31] BODIPY triplet states are commonly non-emissive or possess very weak phosphorescence, limiting the possibility of studying ISC in target dyads by steady-state spectroscopy. To gain better insights into the photophysical processes and excited state dynamics at room temperature, transient absorption (TA) spectroscopy was employed. Based on a photophysical model established earlier in our previous study on **BAD** systems,[20] we expected to observe a series of sequential processes reflected by equations (1)-(4):

$$Excitation\ at\ 355\ nm$$
$$S_0(Pyr) + h\vartheta \rightarrow S_1(Pyr^*) \quad (1)$$

$$Energy\ transfer$$
$$S_1(Pyr^*) \rightarrow S_1(BDP^*) \quad (2)$$

$$Electron\ transfer$$
$$S_1(BDP^*) \rightarrow CT(BDP^{\bullet -} + Pyr^{\bullet +}) \quad (3)$$

$$CT\ \ recombination$$
$$CT(BDP^{\bullet -} + Pyr^{\bullet +}) \rightarrow T_1(BDP^*) \quad (4a)$$

$$CT\ recombination$$
$$CT(BDP^{\bullet -} + Pyr^{\bullet +}) \rightarrow T_1(Pyr^*) \quad (4b)$$

Following excitation at 355 nm, singlet excited states of pyrene (S^{Pyr}) undergo energy transfer (EnT) to the BODIPY core. EnT is followed by photo-induced electron transfer, generating CT states, equivalent to radical ion-pairs composed of pyrene radical-cations ($Pyr^{\bullet+}$) and BODIPY radical-anions ($BDP^{\bullet-}$). The CT states can then undergo recombination to populate triplet excited states of either pyrene (T^{Pyr}) or BODIPY (T^{BDP}).

Figure 8 shows picosecond-nanosecond (ps-ns) TA spectra (panel (a)) and corresponding integrated kinetics of selected spectral regions (panel (b)) of **BPyrD1** in DMF. Pyrene singlet states were created by excitation at 355 nm, the associated decay of the 3.4-3.45 eV band and concomitant rise of the photo bleach (PB) band of BODIPY at 2.45 eV indicates energy transfer (EnT) from pyrene to BODIPY subunits as shown in the inset of panel (a). The population of BODIPY singlet states, following excitation of pyrene at 355 nm and subsequent EnT, was confirmed by steady-state fluorescence experiments, which showed fluorescence mainly from the BODIPY (see Supporting Information, Table S1). Figure 8b shows integrated kinetics of selected spectral regions. Mono-exponential fits on the rise of PB traces (green line) and photo-induced absorption (PA) kinetics (red and blue lines) were performed to obtain kinetic parameters. The fits yielded time constants of 0.31±0.01 ps and 0.49±0.02 ps for EnT and photo-induced electron transfer (PeT), respectively. These values are closely in the range of previous reported values of **BADs**.[22]

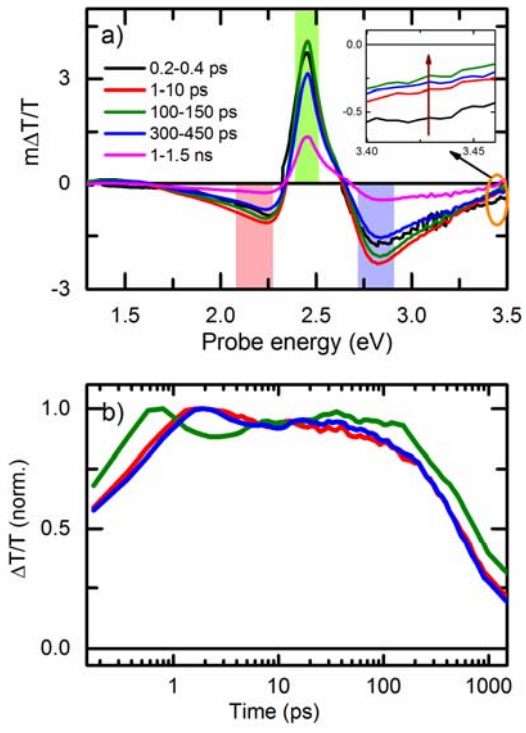

Figure 8. ps-ns Transient absorption spectra of **BPyrD1** in DMF after 355 nm excitation at various delay times as shown in the legend (a). Inset of the panel (a) shows the zoomed-in region belongs to pyrene singlet sates (3.4-3.45 eV) and exhibits an ultrafast decay unlike other spectral regions indicating energy transfer to BODIPY sub-unit. Panel (b) show kinetics of selected spectral regions, as indicated by the vertical color bars in panel (b).

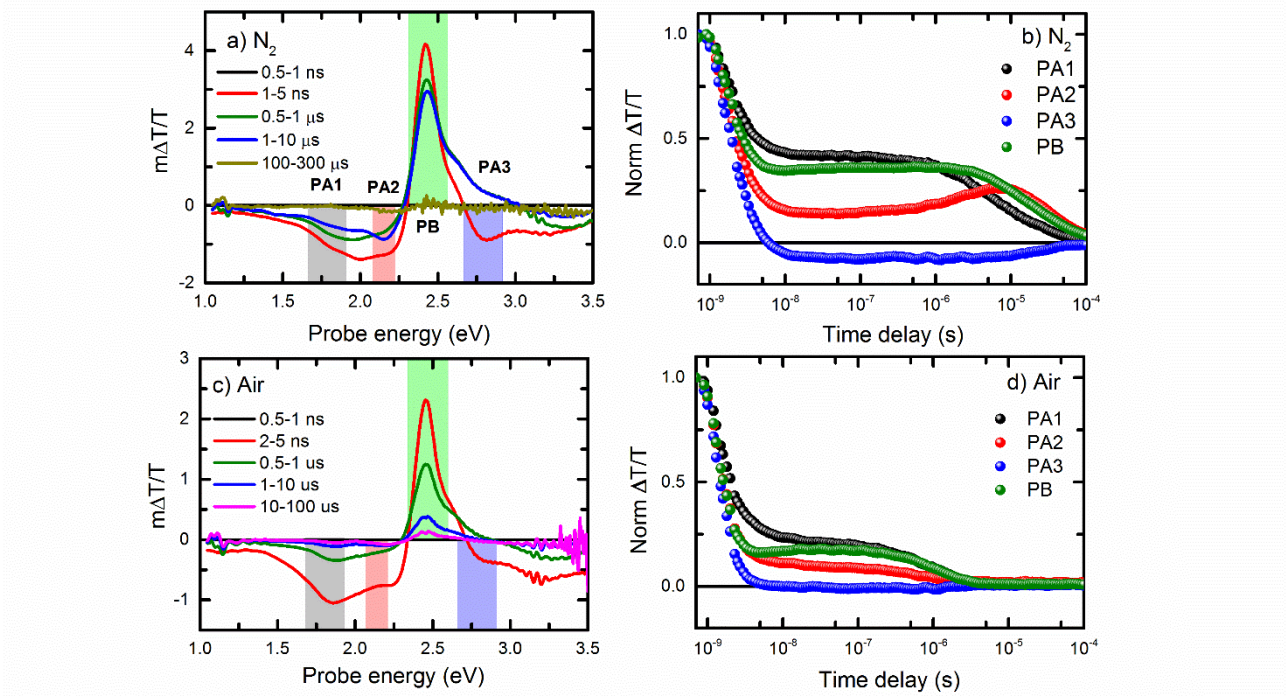

Figure 9. ns-µs TA spectra and kinetics of **BPyrD1** in DMF measured under nitrogen atmosphere (a) and in air (c) at room temperature following excitation at 355 nm with 800 ps pulses at various delay times as indicated in the legend. Panels (b) and (d) show kinetics of the corresponding selected bands, as indicated by vertical color bars in panels (a) and (c), respectively.

To probe the generation and decay of long-lived excited states, we performed separate nanosecond-microsecond TA (ns-µs TA) experiments on **BPyrD1** prepared under nitrogen (Fig. 9a-b) and air (Fig. 9c-d). On the sub-ns timescale, the observed TA spectra were similar to those at shorter delay times (Fig. 8). The TA spectra exhibited rapid spectral changes after a few ns (ca. 5 ns, red line in Fig. 9a) and two clearly distinguishable PA bands peaking at 2.03 eV and 2.75 eV emerged, belonging to the BODIPY radical-anions ($BDP^{\bullet-}$)[17c] and pyrene radical-cations ($Pyr^{\bullet+}$),[32] respectively. At longer delay times (ca. 1 µs), the PA1 band blue-shifted to 2.2 eV (PA2, Fig. 9a) and exhibited a significant rise, indicating the generation of T^{BDP} as previously reported by us and others.[20,33] Figure 9b shows the kinetics of selected spectral regions, as indicated by vertical color bars in Figure 9a. PA2 (triplet band, red symbols) shows a considerable rise after 10 ns, reached the maximum intensity at 10 µs and then started to decay. A mono- exponential growth and decay fit to the PA2 band dynamics yielded inverse rate constants of 2.2 ± 0.05 µs for the triplet generation and 36 ± 0.05 µs for the decay process, respectively. The ns-µs TA spectra of **BPyrD1**, in air (Fig. 9c-d) showed no rise of PA2, but rather exhibited a fast decay due to the quenching of triplet states by oxygen.

To evaluate $^1O_2$ sensitization by the triplet states formed from CT states in the dyads, we studied the trapping of $^1O_2$ with 1,3-diphenylisobenzofuran (DPBF) in polar (ethanol) and non-polar solvents (hexane). Note, that the choice of solvent for trapping experiments is crucially important. In certain cases methods employing DPBF overestimates the $^1O_2$ quantum yields, e.g., due to radicals formation or photolysis of DPBF.[34] This can be seen by a decrease of the DPBF absorption during irradiation in oxygen-free solutions. When ethanol or hexane was employed as solvent no such effect was observed.

Table 3. Quantum yields of singlet oxygen photosensitization by the dyads in ethanol and hexane.[a]

Compound	Φ_Δ, EtOH	Φ_Δ, hexane
8-Phenyl-BODIPY[b]	< 0.01	< 0.01
BPyrD1	0.75±0.11	0.02±0.005
BPyrD2	0.25±0.06	0.01±0.005
BPyrD3	0.34±0.05	0.01±0.005
BPyrD4	0.04±0.001	0.01±0.005
BPyrD5	0.01±0.005	0.01±0.005
BPerD	0.13±0.02	0.01±0.005
BAD1	0.11±0.02	0.39±0.05
BAD2	0.47±0.05	0.07±0.01

[a] Quantum yields were measured using DPBF as a $^1O_2$ trap and Rose Bengal as a reference photosensitizer (0.86 in ethanol). [b] 1,3,5,7-Tetramethyl-8-phenyl-4,4-difluoro-4-bora-3a,4a-diaza-s-indacene.

As shown in Table 3, Φ_Δ values of BODIPY-aryl-dyads largely vary depending on the solvent and subunits structure (for structures of the reference compounds see Fig. 10). The most efficient $^1O_2$ sensitization was observed for **BPyrD1** when ethanol was used as a solvent. This correlates with efficient PeT and triplet state generation observed in the TA experiments.

However, in hexane this dyad showed low Φ_Δ, consistent with the absence of PeT.

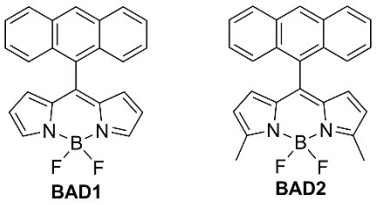

Figure 10. Reference BODIPY-anthracene dyads (BADs).

Dyads **BPyrD2-3**, containing methyl groups, showed lower Φ_Δ values in ethanol (0.25-0.34) and negligible $^1O_2$ sensitization ability in hexane. Furthermore, dyads **BPyrD4-5** showed very low Φ_Δ values in both solvents. For perylene-based dyad **BPerD** a moderate $^1O_2$ sensitization efficiency was observed only in ethanol. To compare the effect of the electron donor moieties in these compounds we included Φ_Δ values of previously studied dyads **BAD1-2** (Fig. 10). Remarkably, **BAD1**, lacking alkyl groups in the BODIPY moiety, showed rather low value of Φ_Δ in ethanol (0.11), but high value in hexane (0.43).

The observed properties raise two questions: 1) why does the triplet yield drop from **BPyrD1** to **BPyrD2** and 2) why is triplet formation not observed for **BPyrD1** in non-polar media, in contrast to **BAD1**? In order to understand the effect of alkyl substituents on PeT in the dyads, a comparative computational study was performed. The size of the studied molecules precluded the use of very accurate excited state methods, such as multireference configuration interaction and multiconfigurational perturbation theory, and hence electronic transitions in the excited state were evaluated using the one-determinant density functional (DFT) approach. Ground electronic state geometries for both **BPyrD1** and **BPyrD2** were optimized in C_s symmetry. Due to the orthogonality of the two fragments, it was possible to achieve SCF convergences of low-lying excited states. For optimized geometries vertical excitation energies were evaluated within the DFT-PCM model[35] for the "local" excited state of the BODIPY fragment (S^{BDP}), and for the charge-transfer states (S^{CT}). All excited states were treated in open-shell singlet variation.

The quantum chemical calculations showed that dyads possessing the same BODIPY scaffold but different electron donors at the bridging 8-position (anthracene or pyrene), exhibit very similar excited state electronic transitions. This is shown in Table 4 with a comparison between the pyrene-based dyads **BPyrD1-2** and reference **BADs 1-2**. The first excited state S^{BDP} of these molecules arises from local $\pi_{BDP}\rightarrow\pi^*_{BDP}$ excitation of BODIPY fragment. After $S_0 \rightarrow S^{BDP}$ excitation, reductive photoinduced electron transfer process from the pyrene (π_{pyr}) to the BODIPY (π_{BDP}) fragments can take place in the S^{BDP} state. In order for PeT processes to occur, it is crucial that the charge-transfer state S^{CT} is energetically close to S^{BDP}. Increasing the energy gap between the states should result in lower yields of CT states.

Table 3. Computed excitation energies for S^{BDP} and S^{CT} states the energy gaps between for **BPerD1-2** and **BAD1-2** in vacuum and ethanol media. All data are given in eV.

	BPyrD1	BAD1	BPyD2	BAD2
$E(S^{BDP})$, vacuum	2.44	2.43	2.33	2.33
$E(S^{BDP})$, vacuum	2.44	2.42	2.33	2.32
$E(S^{CT})$, EtOH	3.16	2.86	3.33	3.03
$E(S^{CT})$, EtOH	2.40	2.18	2.52	2.38
$E(S^{CT}) - E(S^{BDP})$, Vacuum	0.72	0.43	1.00	0.70
$E(S^{CT}) - E(S^{BDP})$, EtOH	–0.04	–0.24	0.19	0.06

The differences in HOMO and LUMO energies given in Figure 4 demonstrates that the introduction of alkyl substituents reduces the electron accepting ability of the BODIPY subunit. Upon PeT, $BDP^{\bullet-}$ species are formed and thus, the addition of alkyl groups increases the energy of the S^{CT} state. In non-polar media, the CT state cannot be fully stabilized *via* dipole-dipole interactions with solvent molecules, resulting in large energy gaps between S^{BDP} and S^{CT} states. High values of $E(S^{CT}) - E(S^{BDP})$, computed for **BPyrD1** in vacuum (0.72 eV), are consistent with low yields of CT states and with very low Φ_Δ found in non-polar hexane. At the same time, for the anthracene-based dyad **BAD1**, the energy gap is substantially decreased (0.43 eV). As a result, the charge-transfer state of **BAD1** can be populated even in non-polar solvents, providing efficient triplet state formation as indicated by high Φ_Δ in hexane (Table 3). Similarly, the large difference in $E(S^{CT}) - E(S^{BDP})$ values between **BPyrD2** and **BAD2** in vacuum is consistent with low Φ_Δ values for these dyads in hexane.

Interactions with polar solvent molecules strongly stabilize CT states, resulting in efficient PeT. In ethanol the S^{CT}/S^{BDP} gap is reduced in **BPyrD1** by ~0.8 eV, while for **BAD1** this change equals ~0.6 eV. This difference is due to the stronger dipole moment of S^{CT} state in **BPyrD1** (~23 D) compared to **BAD1** (~18 D), that leads to more significant stabilization of **BPyrD1** in ethanol media. Population of S^{CT}, in turn, provides efficient triplet state formation and sensitization of $^1O_2$ with a very high quantum yield (0.75). Notably, the singlet oxygen generation of **BAD1** in ethanol was found to be substantially less efficient (0.11). This, in part, can be associated with a larger S^{CT}/S^{BDP} gap in ethanol, compared to **BPyrD1**. On the other hand, reduced triplet state formation for **BAD1** in polar ethanol, compared to non-polar hexane, arises from the sensitivity of the ISC process in this molecule to solvent viscosity, as we found previously.[22]

In polar solvents the $S^{BDP}\rightarrow S^{CT}$ transition can be observed for **BPyrD2** and **BAD2**, bearing methyl groups which destabilize the S^{CT} state. Despite close values of the S^{CT} and S^{BDP} state energies for these dyads in ethanol, a large difference in Φ_Δ values was observed. This indicates the strong influence of the S^{CT}/S^{BDP} gap values on PeT and triplet state formation efficiency. Sufficiently large S^{CT}/S^{BDP} gap in other dyads - due to the effect

of electron-donating alkyl groups - reduce PeT efficiencies both in non-polar and polar solvents.

The destabilizing effect of alkyl groups may account for the very low Φ_Δ value observed for **BPyrD4**, as in this case the low yield of S^{CT} state terminates ISC. We expected that increasing the HOMO orbital energy of the electron donor subunit could compensate this destabilizing effect. Indeed, PeT in dyad **BPerD** was observed to take place with higher efficiency, according to the emission data, resulting in higher Φ_Δ. However, the poor electron accepting ability of this BODIPY scaffold which limits PeT cannot be overcome completely. An alternative possibility in this case would be to combine this BODIPY as an electron donor with an appropriate electron acceptor moiety. This has been previously demonstrated with methylpyridinium and acridinium ion-based BODIPY dyads.[16]

Finally, the fact that in **BPyrD5** triplet state formation was not observed may be associated with the molecular geometry in this dyad. It has been noted in previous works that an orthogonal arrangement of the subunits in multichromophoric systems provides efficient ISC, e.g., in donor-orthogonal-acceptor conjugated polymers[36] and OLED emitters exhibiting thermally-activated delayed fluorescence.[37] Our recent study showed that the orthogonal geometry in **BADs** is responsible for reducing the S-T energy gap in the CT state.[22] In the absence of alkyl substituents at positions 1 and 7 of the BODIPY subunit in these dyads, the molecular geometry can deviate from orthogonality, leading to reduced triplet state yields. The introduction of a phenylene spacer between the subunits, as in **BPyrD5**, results in a molecular geometry with dihedral angles between the subunits of approximately 50°, which minimizes ISC and results in poor triplet state yields, even in the case of efficient PeT.

Conclusions

To conclude, in the **BPyrD** and **BPerD** systems charge transfer was found to mediate the formation of long-lived triplet states as previously observed in **BADs**. PeT in the dyads competes with fluorescence from the BODIPY local excited state. The substitution pattern of the BODIPY and solvent polarity affect the ratio between these processes. Alkyl substituents shift the HOMO energy level of the BODIPY subunit and change the stability of the CT states. Population of CT states leads to the formation of the local BODIPY triplet state T^{BDP}. Thus formed triplets can be used for singlet oxygen generation in polar solvents.

The mechanism of ISC from the CT state to the triplet excited state is not apparent and more detailed studies are necessary to identify whether RP-ISC or SOCT-ISC is the dominant pathway.

The described dyads generate singlet oxygen exclusively in polar media and could be employed as environment-responsive sensitizers in biological environments. Compared to most of the previously reported heavy atom-free BODIPY triplet sensitizers, e.g., symmetrical and unsymmetrical BODIPY dimers,[38] the dyads are easy to access. Adjustment of the substitution pattern in the BODIPY scaffold allows tuning PeT efficiencies and Φ_Δ over a wide range. Notably, it allows for the design of dyads which possess both strong fluorescence and ISC at the same time, such as **BPyrD2-3**. This is an important advantage of these systems, compared to halogenated BODIPYs, which possess high ISC, but are typically poorly emissive.[11]

Experimental Section

General

Pyrene-1-carbaldehyde, pyrrole, 2,4-dimethylpyrrole and 3-ethyl-2,4-dimethylpyrrole were purchased from Sigma-Aldrich. The handling of all air/water sensitive materials was carried out using standard high vacuum techniques. Dried toluene, DCM and THF were obtained by passing through alumina under N_2 in solvent purification systems and then further dried over activated molecular sieves. Dry DMF was purchased from Aldrich. Unless otherwise specified all other solvents were used as commercially supplied. Analytical thin layer chromatography was performed using silica gel 60 (fluorescence indicator F254, pre-coated sheets, 0.2 mm thick, 20 cm × 20 cm; Merck) plates and visualized by UV irradiation (λ = 254 nm). Column chromatography was carried out using Fluka Silica Gel 60 (230–400 mesh).

Spectroscopy

UV-Vis spectra were recorded in solutions using a Specord 250 spectrophotometer from Analytic Jena (1 cm path length quartz cell). Emission, excitation spectra and lifetimes were measured using a Cary Eclipse G9800A fluorescence spectrophotometer and Horiba Jobin Yvon Fluorolog 4 instrument. Emission quantum yields of the compounds were measured relative to the fluorescence of fluorescein in 0.1 M NaOH (φ_f = 0.95).[39] Sample concentrations were chosen to obtain an absorbance of 0.03-0.07, at least three measurements were performed for each sample. NMR spectra were recorded on a Bruker Advance III 400 MHz, a Bruker DPX400 400 MHz or an Agilent 400 spectrometer. Accurate mass measurements (HRMS) were carried out using a Bruker microTOF-Q™ ESI-TOF mass spectrometer. Mass spectrometry was performed with a Q-Tof Premier Waters MALDI quadrupole time-of-flight (Q-TOF) mass spectrometer equipped with Z-spray electrospray ionization (ESI) and matrix assisted laser desorption ionization (MALDI) sources in positive mode with *trans*-2-[3-(4-*tert*-butylphenyl)-2-methyl-2-propenylidene]-malononitrile (DCTB) as matrix. Melting points were measured using an automated melting point meter SMP50 (Stuart) and are uncorrected.

Transient absorption (TA) spectroscopy measurements were carried out using a home-built pump-probe setup. Two different configurations of the setup were used for either short delay, namely 100 fs to 8 ns experiments, or long delay, namely 1 ns to 300 μs delays, as described previously.[22]

Singlet Oxygen Quantum Yield Determinations

The singlet oxygen quantum yield measurements were performed according to a previously described procedure.[20] Solutions of the $^1O_2$ trap, 1,3-diphenylisobenzofuran (DPBF), with an optical density of 1.0 in air-saturated ethanol and hexane were employed. The corresponding dyad was added to the cuvette, and its absorbance was adjusted to around 0.01 at the wavelength of irradiation. The solutions in the cuvette were irradiated with 532 nm laser light at the same power density of 10 mW/cm^2. The absorption spectra of the solutions were measured every 10 s. The slope of plots of absorbance of DPBF at 414 nm *vs.* irradiation time for each photosensitizer was calculated.

Computations

All calculations were performed using GAMESS quantum chemistry package[40] in spin unrestricted formalism using M06-2X meta-GGA functional[41] with 54% of Hartree-Fock exchange part. The Karlsruhe valence triple-zeta KTZV basis set[42] incorporated in GAMESS quantum

chemistry package was employed. Solvent was modeled using iterative isotropic polarizable continuum model (PCM) calculation with parameters corresponding to ethanol.

Syntheses

2-Methylpyrrole,[43] 4-(pyren-1-yl)benzaldehyde[44] and perylene-3-carbaldehyde[45] and **BPyrD1**[46] were prepared according to reported procedures and their analytical data were found to be consistent with those described previously. **BPyrD2-5** and **BPerD** were prepared according to a previously described general procedure.[20]

3,5-Dimethyl-8-(pyren-1-yl)-4,4-difluoro-4-bora-3a,4a-diaza-s-indacene (BPyrD2). Obtained in 19% yield. Red powder, m.p. >300 °C. R_f: 0.42 (DCM-hexane, 1:1). ^{1}H NMR (400 MHz, $CDCl_3$): δ = 8.31 – 8.00 (m, 9H, C$\underline{H}_{Ar}$), 6.42 (d, J=4.0, 2H, C$\underline{H}_{pyrrole}$), 6.22 (d, J=4.1, 2H, C$\underline{H}_{pyrrole}$), 2.74 (s, 6H, C$\underline{H}_3$) ppm. ^{13}C NMR (100 MHz, $CDCl_3$): δ = 158.02, 141.42, 136.12, 132.17, 131.39, 130.91, 130.65, 130.56, 128.71, 128.49, 128.29, 128.04, 127.31, 126.60, 126.01, 125.83, 125.34, 124.61, 124.43, 124.05, 119.78, 15.13 ppm. UV−vis (DCM): λ_{max} [nm] (log ε) = 326 (4.78), 342 (4.61), 516 (4.84). HRMS (ESI): *m/z* found 421.1699, calcd for $[M+H]^+$ $C_{27}H_{20}BN_2F_2$ 421.1686.

1,3,5,7-Tetramethyl-8-(pyren-1-yl)-4,4-difluoro-4-bora-3a,4a-diaza-s-indacene (BPyrD3). Obtained in 19% yield. Analytical data are in correspondence to those described previously.[24]

2,6-Diethyl-1,3,5,7-tetramethyl-8-(pyren-1-yl)-4,4-difluoro-4-bora-3a,4a-diaza-s-indacene (BPyrD4). Obtained in 16% yield. Analytical data are in correspondence to those described previously.[25]

3,5-Dimethyl-8-(4-(10-pyren-1-yl)phenyl))-4,4-difluoro-4-bora-3a,4a-diaza-s-indacene (BPyrD5). Obtained in 13% yield. Orange powder, m.p. >300 °C. R_f: 0.44 (DCM-hexane, 1:1). ^{1}H NMR (400 MHz, $CDCl_3$): δ = 8.28 – 8.16 (m, 4H, C$\underline{H}_{Ar}$), 8.13 – 7.99 (m, 5H, C$\underline{H}_{Ar}$), 7.72 (dd, *J* = 23.8, 7.5 Hz, 4H, C$\underline{H}_{Ar}$), 6.91 (s, 2H, C$\underline{H}_{pyrrole}$), 6.33 (s, 2H, C$\underline{H}_{pyrrole}$), 2.69 (s, 6H, C$\underline{H}_3$) ppm. ^{13}C NMR (100 MHz, $CDCl_3$): δ = 157.62, 143.10, 142.31, 136.37, 134.53, 133.06, 131.45, 130.94, 130.89, 130.36, 130.51, 130.44, 128.38, 127.86, 127.75, 127.49, 127.35, 126.14, 125.37, 125.04, 124.99, 124.84, 124.81, 124.74 , 119.47, 29.68, 14.94 ppm. UV−vis (DCM): λ_{max} [nm] (log ε) = 332 (4.31), 347 (4.42), 513 (4.60). HRMS (ESI): *m/z* found 497.1997, calcd for $[M+H]^+$ $C_{33}H_{24}BF_2N_2$ 497.2000.

2,6-Diethyl-1,3,5,7-tetramethyl-8-(perylen-3-yl)-4,4-difluoro-4-bora-3a,4a-diaza-s-indacene (BPerD). Obtained in 21% yield. Red powder, m.p. >300 °C. R_f: 0.27 (DCM-hexane, 1:1). ^{1}H NMR (400 MHz, $CDCl_3$): δ = 8.32 – 8.21 (m, 4H, C$\underline{H}_{Ar}$), 7.74 (t, *J* = 7.5 Hz, 2H, C$\underline{H}_{Ar}$), 7.67 (d, *J* = 8.3 Hz, 1H, C$\underline{H}_{Ar}$), 7.53 (td, *J* = 7.8, 5.4 Hz, 2H, C$\underline{H}_{Ar}$), 7.47 – 7.37 (m, 2H, C$\underline{H}_{Ar}$), 2.58 (s, 6H, C$\underline{H}_3$), 2.27 (q, *J* = 7.5 Hz, 4H, C$\underline{H}_2$), 1.19 (s, 6H, C$\underline{H}_3$), 0.96 (t, *J* = 7.5 Hz, 6H, C$\underline{H}_3$) ppm. ^{13}C NMR (100 MHz, $CDCl_3$): δ = 153.98, 138.40, 138.22, 134.77, 133.44, 132.88, 132.80, 132.28, 131.42, 131.23, 131.00, 130.74, 128.85, 128.62, 128.51, 128.24, 127.70, 126.98, 126.81, 126.68, 125.19, 120.84, 120.70, 120.69, 120.13, 17.08, 14.64, 12.62, 11.45 ppm. UV−vis (DCM): λ_{max} [nm] (log ε) = 418 (4.59), 446 (4.63), 531 (5.01). HRMS (ESI): *m/z* found 535.2702, calcd for $[M-F]^+$ $C_{37}H_{33}BN_2F$ 535.2721.

X-ray Crystallography

X-ray diffraction data for all compounds were collected on a Bruker APEX 2 DUO CCD diffractometer by using graphite-monochromated MoK_α (λ = 0.71073 Å) radiation or Incoatec IμS CuK_α (λ = 1.54178 Å) radiation. Crystals were grown by liquid diffusion of a solution of the compounds in CH_2Cl_2 and MeOH.[47] Crystals were mounted on a MiTeGen MicroMount and collected at 100(2) K using an Oxford Cryosystems Cobra low-temperature device. Data was collected by using omega and phi scans and are corrected for Lorentz and polarization effects by using the APEX software suite.[48] Using Olex2, the structure was solved with the XT structure solution program, using the intrinsic phasing solution method and refined against $|F^2|$ with XL using least squares minimization.[49] Hydrogen atoms were generally placed in geometrically calculated positions and refined using a riding model. Full details of data refinements are given in the supplementary material and Table S2. All images were prepared by using Olex2.

Crystal Data for BPyrD1: $C_{25}H_{15}BF_2N_2$ (*M* =392.20 g/mol): monoclinic, space group $P2_1/c$ (no. 14), *a* = 17.082(17) Å, *b* = 8.600(12) Å, *c* = 13.632(14) Å, *β* = 112.854(15)°, *V* = 1845(4) Å^3, *Z* = 4, *T* = 100.01 K, μ(MoK_α) = 0.097 mm^{-1}, D_{calc} = 1.412 g/cm^3, 19468 reflections measured (5.176° ≤ 2θ ≤ 59.246°), 5178 unique (R_{int} = 0.0330, R_{sigma} = 0.0328) which were used in all calculations. The final R_1 was 0.0413 (I > 2σ(I)) and wR_2 was 0.1142 (all data).

Crystal Data for BPyrD3: $C_{29}H_{23}BF_2N_2$ (*M* =448.30 g/mol): orthorhombic, space group $P2_12_12_1$ (no. 19), *a* = 8.5915(4) Å, *b* = 11.3514(6) Å, *c* = 23.2887(11) Å, *V* = 2271.24(19) Å^3, *Z* = 4, *T* = 99.99 K, μ(MoK_α) = 0.087 mm^{-1}, D_{calc} = 1.311 g/cm^3, 92743 reflections measured (3.498° ≤ 2θ ≤ 62.28°), 7314 unique (R_{int} = 0.0651, R_{sigma} = 0.0303) which were used in all calculations. The final R_1 was 0.0408 (I > 2σ(I)) and wR_2 was 0.0981 (all data). The methyl groups at the α-positions (C3 and C5) and the β-positions (C1 and C7) were modelled in two positions using restraints (ISOR, SADI, and DFIX) and constraint (EDAP) in a 90:10 % occupancy.

Crystal Data for BPyrD4: $C_{33}H_{31}BF_2N_2$ (*M* =504.41 g/mol): monoclinic, space group *Cc* (no. 9), *a* = 7.8654(2) Å, *b* = 44.0642(11) Å, *c* = 14.9251(4) Å, *β* = 91.213(2)°, *V* = 5171.6(2) Å^3, *Z* = 8, *T* = 99.99 K, μ(CuK_α) = 0.676 mm^{-1}, D_{calc} = 1.296 g/cm^3, 60945 reflections measured (4.01° ≤ 2θ ≤ 135.99°), 9342 unique (R_{int} = 0.0505, R_{sigma} = 0.0311) which were used in all calculations. The final R_1 was 0.0392 (I > 2σ(I)) and wR_2 was 0.1063 (all data). Two individual data collections on one crystal were merged together to get complete data for this structure. The overall structure was refined as a two-component inversion twin.

Crystal Data for BPerD: $C_{37}H_{33}BF_2N_2$ (*M* =554.46 g/mol): monoclinic, space group $P2_1/n$ (no. 14), *a* = 7.8092(3) Å, *b* = 30.8205(11) Å, *c* = 23.4106(9) Å, *β* = 95.314(2)°, *V* = 5610.3(4) Å^3, *Z* = 8, *T* = 100.01 K, μ(CuK_α) = 0.675 mm^{-1}, D_{calc} = 1.313 g/cm^3, 48297 reflections measured (4.752° ≤ 2θ ≤ 136.504°), 10233 unique (R_{int} = 0.0685, R_{sigma} = 0.0577) which were used in all calculations. The final R_1 was 0.0949 (I > 2σ(I)) and wR_2 was 0.2740 (all data). The perylene unit to the second residue was modelled over two positions to using restraints (ISOR and SADI) and constraints (EADP) in a 50:50 % occupancy. The boron difluoride moiety of residue two was modeled over two positions in a 87:13 % occupancy.

CCDC 1819150–1819153 contain the supplementary crystallographic data for this paper. These data can be obtained free of charge from The Cambridge Crystallographic Data Centre *via* www.ccdc.cam.ac.uk/data_request/cif.

Acknowledgements

This work was supported by grants from the European Commission (CONSORT, Grant No. 655142), Science Foundation Ireland (SFI IvP 13/IA/1894) and the Irish Research Council (GOIPG/2016/1250). The research reported in this publication was supported by funding from King Abdullah University of Science and Technology (KAUST).

Keywords: photo-induced electron transfer • charge-transfer state • triplet excited state • heavy atom-free sensitizer • singlet oxygen

[1] a) G. N. Lewis, M. Kasha, *J. Am. Chem. Soc.* **1944**, *66*, 2100–2116; b) M. Kasha, *Chem. Rev.* **1947**, *41*, 401–419.

[2] S. B. Brown, E. A. Brown, I. Walker, *Lancet Oncol.* **2004**, *5*, 497–508.

[3] R. C. Evans, P. Douglas, C. J. Winscom, *Coord. Chem. Rev.* **2006**, *250*, 2093–2126.

[4] D. M. Arias-Rotondoa, J. K. McCusker, *Chem. Soc. Rev.* **2016**, *45*, 5803–5820.

[5] X.-D. Wang, O. S. Wolfbeis, *Chem. Soc. Rev.* **2014**, 43, 3666–3761.
[6] J. Zhou, Q. Liu, W. Feng, Y. Sun, F. Li, *Chem. Rev.* **2015**, *115*, 395–465.
[7] J. Zhao, W. Wu, J. Sun, S. Guo, *Chem. Soc. Rev.* **2013**, *42*, 5323–5351.
[8] M. R. Wasielewski, *Chem. Rev.* **1992**, *92*, 435–461.
[9] K. Hasharoni, H. Levanon, S. R. Greenfield, D. J. Gosztola, W. A. Svec, M. R. Wasielewski, *J. Am. Chem. Soc.* **1996**, *118*, 10228–10235.
[10] M. A. El-Sayed, *J. Chem. Phys.* **1974**, *60*, 4502−4507.
[11] a) A. Loudet, K. Burgess, *Chem. Rev.* **2007**, *107*, 4891−4932; b) G. Ulrich, R. Ziessel, A. Harriman, *Angew. Chem. Int. Ed.* **2008**, *47*, 1184–1201.
[12] T. Kowada, H. Maeda, K. Kikuchi, *Chem. Soc. Rev.* **2015**, *44*, 4953−4972.
[13] W. Wu, J. Sun, X. Cui, J. Zhao, *J. Mater. Chem. C* **2013**, *1*, 4577–4589.
[14] W. Wu, J. Zhao, J. Sun, S. Guo, *J. Org. Chem.* **2012**, *77*, 5305–5312.
[15] A. C. Benniston, G. Copley, H. Lemmetyinen, N. V. Tkachenko, *ChemPhysChem* **2010**, *11*, 1685–1692.
[16] a) A. Harriman, L. J. Mallon, G. Ulrich, R. Ziessel, *ChemPhysChem* **2007**, *8*, 1207–1214; (b) X. He, A. C. Benniston, H. Lemmetyinen, N. V. Tkachenko, *ChemPhotoChem,* doi: 10.1002/cptc.201700184.
[17] a) X.-F. Zhang, X. Yang, B. Xu, *Phys. Chem. Chem. Phys.* **2017**, *19*, 24792–24804; b) N. Epelde-Elezcano, E. Palao, H. Manzano, A. Prieto-Castañeda, A. R. Agarrabeitia, A. Tabero, A. Villanueva, S. de la Moya, I. López-Arbeloa, V. Martínez-Martínez, M. J. Ortiz, *Chem. Eur.* J. **2017**, *23*, 4837–4848; c) L. Ya, J. Zhao, A. Iagatti, L. Bussotti, P. Foggi, E. Castellucci, M. Di Donato, K.-L. Han, *J. Phys. Chem. C* **2018**, doi: 10.1021/acs.jpcc.7b10213.
[18] a) K. Liu, R. A. Lalancette, F. Jäkle, *J. Am. Chem. Soc.* **2017**, *139*, 18170–18173; b) F. Boscá, M. C. Cuquerella, V. F. Pais, A. Ros, U. Pischel, *ChemPhotoChem* **2018**, *2*, 34–41.
[19] a) T. Yogo, Y. Urano, Y. Ishitsuka, F. Maniwa, T. Nagano, *J. Am. Chem. Soc.* **2005**, *127*, 12162–12163; b) A. Kamkaew, S. H. Lim, H. B. Lee, L. V. Kiew, L. Y. Chung, K. Burgess, *Chem. Soc. Rev.* **2013**, *42*, 77–88.
[20] M. A. Filatov, S. Karuthedath, P. M. Polestshuk, H. Savoie, K. J. Flanagan, C. Sy, E. Sitte, M. Telitchko, F. Laquai, R. W. Boyle, M. O. Senge, *J. Am. Chem. Soc.* **2017**, *139*, 6282–6285.
[21] N. Kiseleva, M. A. Filatov, M. Oldenburg, D. Busko, M. Jakoby, I. A. Howard, B. S. Richards, M. O. Senge, S. M. Borisov, A. Turshatov, *Chem. Commun.* **2018**, *54*, 1607–1610.
[22] M. A. Filatov, S. Karuthedath, P. M. Polestshuk, S. Callaghan, K. J. Flanagan, M. Telitchko, T. Wiesner, F. Laquai, M. O. Senge, *Phys. Chem. Chem. Phys.* **2018**, in press, doi 10.1039/C7CP08472B.
[23] C. Caltagirone, M. Arca, A. M. Falchi, V. Lippolis, V. Meli, M. Monduzzi, T. Nylander, A. Rosa, J. Schmidt, Y. Talmon, S. Murgia, *RSC Adv.* **2015**, *5*, 23443–23449.
[24] a) Y. Yang, L. Zhang, C. Gao, L. Xu, S. Bai, X. Liu, *RSC Adv.* **2014**, *4*, 38119–38123; b) F. Bizet, M. Ipuy, Y. Bernhard, V. Lioret, P. Winckler, C. Goze, J.-M. Perrier-Cornet, R. A. Decréau, *Bioorg. Med. Chem.* **2018**, *26*, 413–420.
[25] J. P. Rostron, G. Ulrich, P. Retailleau, A. Harriman, R. Ziessel, *New J. Chem.* **2005**, *29*, 1241–1244.
[26] S. Mukherjee, P. Thilagar, *RSC Adv.* **2015**, *5*, 2706–2714.
[27] R. W. Wagner, J. S. Lindsey, *Pure Appl. Chem.* **1996**, *68*, 1373–1380.
[28] a) J. Li, Y. Qian, L. Xie, Y. Yi, W. Li, W. Huang *J. Phys. Chem. C* **2015**, *119*, 2133–2141; b) Y. Qian, M. Cai, X. Zhou, Z. Gao, X. Wang, Y. Zhao, X. Yan, W. Wei, L. Xie, W. Huang, *J. Phys. Chem. C* **2012**, *116*, 12187–12195.
[29] M. Maus, W. Rettig, *J. Phys. Chem. A* **1999**, *103*, 3388–3401.
[30] G. J. Kavarnos, N. J. Turro, *Chem. Rev.* **1986**, *86*, 401–449.
[31] M. T. Whited, P. I. Djurovich, S. T. Roberts, A. C. Durrell, C. W. Schlenker, S. E. Bradforth, M. E. Thompson, *J. Am. Chem. Soc.* **2011**, *133*, 88–96.
[32] a) A. D'Aléo, E. Cecchetto, L. De Cola, R. M. Williams, *Sensors* **2009**, 9, 3604–3626; b) M. S. Altamirano, C. M. Previtali, *J. Photochem. Photobiol. A:Chem.* **2015**, *310*, 165–170; c) T. M. Safko, S. Jiang, L. Zhang, Q. Zhang, R. G. Weiss, *Photochem. Photobiol. Sci.* **2017**, *16*, 972–984.
[33] Z. Wang, J. Zhao, *Org. Lett.* **2017**, *19*, 4492–4495.
[34] X.-F. Zhang, X. Li, J. Lumin., **2011**, *131*, 2263–2266.
[35] H. Li, C. S. Pomelli, J. H. Jensen, *Theor. Chem. Acc.* **2003**, *109*, 71–84.
[36] D. M. E. Freeman, A. J. Musser, J. M. Frost, H. L. Stern, A. K. Forster, K. J. Fallon, A. G. Rapidis, F. Cacialli, I. McCulloch, T. M. Clarke, R. H. Friend, H. Bronstein, *J. Am. Chem. Soc.* **2017**, *139*, 11073–11080.
[37] F. B Dias, J. Santos, D. R. Graves, P. Data, R. S. Nobuyasu, M. A. Fox, A. S. Batsanov, T. Palmeira, M. N. Berberan-Santos, M. R. Bryce, A. P. Monkman, *Adv. Sci.* **2016**, 1600080.
[38] S. Duman, Y. Cakmak, S. Kolemen, E. U. Akkaya, Y. Dede, *J. Org. Chem.* **2012**, *77*, 4516–4527.
[39] J. R. Lakowicz, *Principles of Fluorescence Spectroscopy*, 2nd Ed., Kluwer Academic/Plenum Publishers, New York, London, Moscow, Dordrecht, **1999**, pp. 63–94.
[40] M. W. Schmidt, K. K. Baldridge, J. A. Boatz, S. T. Elbert, M. S. Gordon, J. H. Jensen, S. Koseki, N. Matsunaga, K. A. Nguyen, S. Su, T.L. Windus, M. Dupuis, J. A. Montgomery, *J. Comput. Chem.* **1993**, *14*, 1347–1363.
[41] Y. Zhao, D.G. Truhlar, *Theor. Chem. Acc.* **2006**, *120*, 215–241.
[42] A. Schäfer, H. Horn, R. Ahlrichs, *J. Chem. Phys.* **1992**, *97*, 2571–2577.
[43] P. A. Liddell, T. P. Forsyth, M. O. Senge, K. M. Smith, *Tetrahedron* **1993**, *49*, 1343–1350.
[44] A. Kathiravan, V. Srinivasan, T. Khamrang, M. Velusamy, M. Jaccob, N. Pavithra, S. Anandan, K. Velappan, *Phys. Chem. Chem. Phys.* **2017**, *19*, 3125–3135.
[45] Z. Mahmood, J. Zhao, *J. Org. Chem.* **2016**, *81*, 587–594.
[46] C. Caltagirone, M. Arca, A. M. Falchi, V. Lippolis, V. Meli, M. Monduzzi, T. Nylander, A. Rosa, J. Schmidt, Y. Talmon, S. Murgia, *RSC Adv.* ***2015***, *5*, 23443–23449.
[47] a) H. Hope, *Progr. Inorg. Chem.* **1994**, *41*, 1–19; b) M. O. Senge, *Z. Naturforsch.* **2000**, *55b*, 336–344.
[48] a) *SAINT*, version 8.34a, Bruker AXS, Inc.; Madison, WI, 2013; b) *SADABS*, version 2014/5, Bruker AXS, Inc.; Madison, WI, 2014; c) *APEX2*, version 2014.11-0, Bruker AXS, Inc.; Madison, WI, 2014.
[49] a) O. V. Dolomanov, L. J. Bourhis, R. J. Gildea, J. A. K. Howard, H. Puschmann, *J. Appl. Cryst.* **2009**, *42*, 339–341; b) G. M. Sheldrick, *Acta Cryst.* **2015**, *A71*, 3–8.

Entry for the Table of Contents

ARTICLE

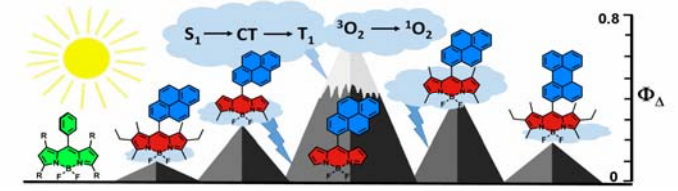

Efficient intersystem crossing in BODIPY electron donor-acceptor dyads is reported. Unlike conventional chromophores, in which triplet states formation relies on heavy atoms and is pre-determined by the chemical structure of the molecule, fluorescence and ISC in the dyads studied can be adjusted by the media polarity.

Dr. Mikhail A. Filatov, Dr. Safakath Karuthedath, Dr. Pavel M. Polestshuk, Susan Callaghan, Thomas Wiesner, Keith J. Flanagan, Prof. Dr. Frédéric Laquai and Prof. Dr. Mathias O. Senge**

Page No. – Page No.

BODIPY-pyrene and perylene dyads as heavy atom-free singlet oxygen sensitizers